Manuscript for *Revista Mexicana de Astronomía y Astrofísica* (2007)

QUARK NOVA SIGNATURES IN SUPER-LUMINOUS SUPERNOVAE

M. Kostka,[1] N. Koning,[1] D. Leahy, [1] R. Ouyed,[1] and W. Steffen,[2]

Draft version: February 27, 2014

RESUMEN

ABSTRACT

In this work we study the light curves of eight super-luminous supernovae (SLSNe) in the context of dual-shock quark novae. The best fit values for progenitor star masses fall in the range of 25-35 $M_{\odot}$ for all SLSNe light curves studied. An examination into the effects of varying the physical properties of a dual-shock quark nova on light curve composition is undertaken. We conclude that the wide variety of SLSN light curve morphologies can be explained predominantly by variations in the length of time between supernova and quark nova. The Hα spectral profile of the dual-shock quark nova is compared to the Hα line observed in three SLSN spectra. Predictions of dual-shock quark nova spectral signatures are presented.

Key Words: Dense matter — Neutron stars — (Stars:) supernovae: individual: 2005ap, 2006tf, 2006gy, 2007bi, 2008es, 2008fz, PTF09cnd, PTF10cwr (2010gx)

1. INTRODUCTION

The standard astrophysical explanation for a supernova (SN) is that the radiated power is generated by energy deposited in an expanding ejecta through one of three mechanisms: the SN shock travels through the stellar envelope (Grassberg et al. 1971), radioactive decay of heavy elements synthesized in the explosion (Arnett 1982) or a collision with hydrogen-rich circumstellar material (CSM) (Chevalier 1982). In 2011 astronomers working on the Palomar Transient Factory announced the emergence of a new class of SNe that cannot be explained by any of these means (Quimby et al. 2011). As described by Quimby et al. (2011) this new class of super-luminous SNe (SLSNe) displays spectra with little to no hydrogen, emits significant UV flux over a long period of time and has a late stage luminosity evolution that is inconsistent with radioactive decay.

While this hydrogen-poor class of SLSNe is recent admission, the phenomenon of SLSNe as a whole has been an open question since the discovery of SN 2006gy (Quimby et al. 2007b). Large scale supernovae surveys such as the Palomar Transient Factory (PTF) (Rau et al. 2009; Law et al. 2009), the

[1]Department of Physics and Astronomy, University of Calgary, Calgary, AB, Canada, T2N 1N4

[2]Instituto de Astronomía Universidad Nacional Autonoma de México, Ensenada, B.C., Mexico

ROTSE Supernova Verification Project (RSVP, formerly the Texas Supernova Search) (Quimby et al. 2005) and the Catarina Real-Time Transient Survey (Drake et al. 2009) have uncovered approximately ten other SLSNe, some of which contain hydrogen in their spectra (SN 2006gy (Quimby et al. 2007b), SN 2008fz (Drake et al. 2010)) while others are hydrogen-poor (SN 2005ap (Quimby et al. 2007b), SN 2007bi (Gal-Yam et al. 2009)).

One method being considered to power the radiated energy of some SLSNe is a scaled up version of a CSM interaction. A dense, massive ($\sim 20 M_\odot$) CSM envelope enshrouds the progenitor star at the time of SN explosion. An efficient conversion of SN kinetic energy to radiation via the SN shock powers the SLSN light curve (Smith et al. 2008; Chevalier & Irwin 2011; Ginzburg & Balberg 2012; Kiewe et al. 2012). Building such a CSM envelope requires a mass-loss rate of $\dot{M} > 0.1 M_\odot$ yr^{-1} over the final 10-100 years prior to SN explosion (Moriya et al. 2013; Ginzburg & Balberg 2012). Two possible explanations for a mass-loss rate on this order are LBV-like mass ejections (Smith et al. 2008; Kiewe et al. 2012) or common envelope phase of an interacting binary system (Chevalier 2012).

An alternative description considered for SLSNe is that the radiated energy is converted from the rotational energy of a magnetar (Kasen & Bildsten 2010; Woosley 2010) inside a SN envelope. For the magnetar model to power the light curve of a SLSN, large PdV losses must be avoided by delaying the conversion of the magnetar's rotational energy into radiation. An explanation for the delay in energy injection has yet to be examined. The delayed injection of energy into the SN envelope must be isotropically distributed across the inner edge of the SN envelope energizing the entire envelope and generating the radiated energy of a SLSN. Whether the magnetar model can power a SLSN with the expected jet-like (Bucciantini et al. 2009) energy deposition has yet to be studied. Dessart et al. (2012) provided an indicative study into the magnetar model explanation for the observed blue spectrum and broad spectral lines seen in most SLSNe.

Pair-instability SNe (PISNe) have as well been proposed as the underlying energy mechanism for SLSNe. In this scenario an extremely massive star becomes prone to $\gamma = 4/3$ instability, triggering a SN explosion. Pan et al. (2012) studied the progenitor stars for PISN and found that the mass range required for a star to end its life as a PISN is $\sim 300 - 1000 M_\odot$. The predicted light curve from a PISN should be nearly symmetric (Kawabata et al. 2009; Dessart et al. 2012).

Ouyed et al. (2002) suggested that a collision between material ejected through the quark nova (QN) explosion of a neutron star and the preceding SN envelope could rebrighten the SN (see section 5.4 of Ouyed et al. (2002)). This theory was first applied in the context of SLSNe by Leahy & Ouyed (2008) to explain SN 2006gy. Table 1 summarizes each proposed model's explanation for a variety of SLSNe characteristics. While acknowledging that other models are being pursued to explain SLSNe, in this work we provide the QN as a possible engine for a universal explanation for SLSNe. Observations of the

SLSNe studied in this work are introduced in section 2. Section 3 summarizes the explosion mechanism of the QN as well as the environment which leads to a SLSN. Section 4 examines the physics implemented in describing the interaction between ejecta of a SN and a QN. Analysis of the effects of changing physical parameters on our model light curve is undertaken in section 5. In section 6 we compare observations of eight SLSNe (SN 2005ap, SN 2006gy SN 2006tf, SN 2007bi, SN 2008es, SN 2008fz, PTF09cnd and PTF10cwr) to QNe of different physical parameters. A discussion of trends found fitting the SLSNe and spectral analysis for some targets is presented in section 7. Finally our conclusions as well as predicted chemical signatures of our model are discussed in section 8.

2. OBSERVATIONS

For this analysis we have chosen eight SLSNe (SN 2005ap, SN 2006gy, SN 2006tf, SN 2007bi, SN 2008es, SN 2008fz, PTF09cnd and PTF10cwr) to study in the context of the quark nova (Ouyed et al. 2002). Each SLSN target along with the peak magnitude, class and proposed models are summarized in Table 2. The SLSNe studied in this work fall into a variety of types. SN 2005ap, PTF09cnd and PTF10cxr are members of a newly identified hydrogen-poor superluminous class of SNe (Quimby et al. 2011). SN 2006gy, SN 2006tf and SN 2008fz have been identified as type IIn SNe as their spectra contain narrow hydrogen emission lines. SN 2007bi is identified as a type Ic SN as its spectrum lacks hydrogen and both the silicon 6355 Angstrom and helium 5876 Angstrom lines. SN 2008es was identified as a type II-L SN due to the presence of hydrogen in its spectrum and the linear decay of its light curve. With the aforementioned transient surveys the number of observed SLSNe is growing steadily and it is not feasible to model all of them. This subset of SLSNe was chosen because as a group they span the range of observed SLSN light curve morphologies.

The first SLSN ever observed was SN 2006gy (Quimby et al. 2007b) which peaked in absolute R band magnitude at approximately -22. The spectrum of SN 2006gy is dominated by a broad Hα emission line (Smith et al. 2010) and while SN 2006gy was exceptionally bright in visible light the event was surprisingly quiet in X-rays (Smith & McCray 2007).

Spurred by the discovery of SN 2006gy, Quimby et al. (2007b) found another extremely bright (-22.7 peak absolute R-band magnitude) SN 2005ap; which remains the brightest SLSN ever observed. The spectrum of SN 2005ap shows broad spectral lines (Hα, C III, N III) and similar to SN 2006gy, SN 2005ap was quiet in X-rays (Quimby et al. 2007b).

SN 2006tf was discovered by Quimby et al. (2007a) who noted that the spectrum closely resembles that of SN 2006gy. Observations of the light curve of SN 2006tf missed the leading edge of the SLSN and thus the actual peak magnitude is unclear, however the total radiated energy of the SLSN was at least 7×10^{50} ergs (Smith et al. 2008). Smith et al. (2007) noted that the light curve of SN 2006tf is characterized by a very slow luminosity decay rate

(~ 0.01 Mag. day^{-1}). The spectra of SN 2006tf displays a strong Hα emission line that remains broad over time (Smith et al. 2008). Hα and Hβ show an interesting evolution in which the red-side of the profile remains constants while the blue-side emission wing becomes more prominent with time (Smith et al. 2008). There exists a blue-side absorption feature seen in He I λ5876 and O I λ7774 that is of comparable width to the blue-side absorption feature of Hα (Smith et al. 2008).

Gal-Yam et al. (2009) discovered the SLSN SN 2007bi and identified it as a type Ic SN, noting that there was no sign of a CSM interaction. The light curve of SN 2007bi peaks at ~ -21.3 in the R band and displays a slow luminosity decay rate (~ 0.01 Mag. day^{-1}) (Gal-Yam et al. 2009). As discussed by Young et al. (2010), the relatively high host galaxy metalicity is inconsistent with a PISN explanation for the SLSN. The slowly evolving spectra of SN 2007bi shows strong oxygen and iron lines (Young et al. 2010).

Discovered by Gezari et al. (2009), the light curve of SN 2008es peaks at ~ -22.2 in the R band and shows a fast luminosity decay rate (~ 0.042 Mag. day^{-1}). The total radiated energy in UV and visible is in excess of 10^{51} ergs, however consistent with other SLSN, SN 2008es was quiet in X-rays (Gezari et al. 2009). The spectrum of SN 2008es is dominated by broad features that lack the narrow and intermediate width line emission typically associated with a CSM interaction (Miller et al. 2009). The spectral evolution of SN 2008es shows that the broad components of the spectral lines become more prominent over time (Miller et al. 2009).

SN 2008fz was discovered by Drake et al. (2010) who found the light curve to peak at ~ -22.3 in the V band and shows a similar slow evolution to that of SN 2006gy. The spectrum of SN 2008fz displays strong Balmer lines that are initially narrow but become broad over time, Drake et al. (2010) noted that the Hα emission line of SN 2008fz is similar to that of SN 2006gy for the same epoch.

We chose to study PTF09cnd and PTF10cwr as representative members of the new hydrogen-poor SLSN class (Quimby et al. 2011). These SLSNe were selected because they display the two extremes of light curve morphology for this class, PTF09cnd has the brightest and broadest u-band light curve in the class and PTF10cwr the dimmest and narrowest.

The luminosity decay rate of both PTF09cnd and PTF10cwr are inconsistent with radioactive decay and the spectrum shows no signs of a CSM interaction (Quimby et al. 2011). PTF10cwr was also observed in the B band by Pastorello et al. (2010), in which it peaks at ~ -21.2, and alternatively is referred to as SN 2010gx. As mentioned in the supplemental material associated with Quimby et al. (2011), the SLSNe PTF09cnd and PTF10cwr are quiet in X-rays relative to the amount of energy radiated in the visual bands.

3. QUARK NOVA

The idea that nuclei could collapse into constitute quark matter and the possible existence of quark stars have been theorized for several decades (Itoh

1970; Bodmer 1971). Witten (1984) conjectured that up-down-strange *(u,d,s)* quark matter is a state of matter more stable than ^{56}Fe. Within the hypothesis that *(u,d,s)* matter is the true ground state of hadrons the proposition that a neutron star could convert to a *(u,d,s)* quark star was put forth by Alcock et al. (1986). They detailed numerous possible mechanisms for achieving the requisite strangeness to convert a neutron star into a quark star. Different astrophysical scenarios which could achieve this phase transition have been speculated. One such possibility is during or shortly after a SN when the core density of the proto-neutron star is high enough to trigger quark deconfinement (Dai et al. 1995; Xu et al. 2001). Another candidate involves converting a neutron star to a quark star (Olinto 1987; Cheng & Dai 1996; Bombaci & Datta 2000). The final result from this phase transition is still being debated. Some hydrodynamic simulations show that the phase transition will halt because the transition is no longer exothermic, resulting in a hybrid star (Herzog & Röpke 2011). In other studies the entire neutron star is converted to a quark star within milliseconds providing a powerful source of neutrinos (Pagliara et al. 2013). For this work we will assume the scenario in which the *(u,d)* quark matter core of a hybrid star (Alcock et al. 1986) contracts during the conversion to *(u,d,s)* quark matter such that a physical separation between the core and the overlaying neutron star material develops, as proposed by Ouyed et al. (2002) which introduced the concept of the QN.

In the QN scenario dense neutron-rich material is ejected during the conversion from a neutron star to a quark star. Mechanisms for powering the mass ejection will be discussed in section 3.1. The ultra-high density of the quark star remnant implies that the color-superconducting color-flavour locked (CFL) phase is favoured (Alford et al. 1999).

In the CFL phase the density is sufficiently high such that the mass of the strange quark can be neglected and up, down, and strange quarks can be treated equally (Alford et al. 2008, and references therein). All three colors and flavours of quarks in the CFL phase condense into zero-momentum, spinless Cooper pairs (Srednicki & Susskind 1981; Alford et al. 1999) with zero net charge, a pairing pattern that breaks chiral symmetry. The CFL condensates are not invariant under color nor flavour rotations, but only under simultaneous color and flavour rotations, hence the color-flavour locking (Alford et al. 1999). Low energy excitations relevant to the interior of compact objects for matter in the CFL phase are characterized by Goldstone modes; a nearly massless octet and a singlet of Goldstone bosons associated with the breaking of chiral and axial symmetry and a massless Goldstone boson associated breaking of baryon number symmetry (Jaikumar et al. 2002). The presence of massless Goldstone bosons cause CFL matter to be a superfluid (Son & Stephanov 2000a,b; Son 2002). Neutrino emission relevant to long-term cooling of CFL stars (temperatures in the sub-MeV range) was studied by Jaikumar et al. (2002). Reddy et al. (2003a,b) studied neutrino emission from a CFL star at temperatures up to 30 MeV, the hottest phases expected for the early evolution of a proto-neutron star (e.g. Shapiro & Teukolsky 1983).

Photon emission from a CFL star at temperatures in the tens of MeV range was studied by Vogt et al. (2004).

3.1. *Explosion Mechanism*

The QN converts gravitational energy and nuclear binding energy into internal energy (heat) and partially into kinetic energy. Several possible mechanisms for powering mass ejection during a QN have been studied.

Keränen et al. (2005) studied possible QN mass ejection powered by neutrinos generated during the phase transition from *(u,d)* to *(u,d,s)* quark matter (Iwamoto 1980; Dai et al. 1995). Since the diffusion timescale for neutrinos in *(u,d,s)* matter is long enough to thermalize (∼10-100 ms) most neutrinos are trapped within the *(u,d,s)* core (Keränen et al. 2005). If a small fraction of these neutrinos escape the *(u,d,s)* core before the entire neutron star is converted they can transport enough energy into the outer regions of the star to be capable of causing a wind-like mass ejection of $\sim 10^{-5} - 10^{-2} M_{\odot}$ (Keränen et al. 2005).

A more attractive alternative to neutrino-driven ejection is that mass ejection in a QN is powered by a photon fireball that builds up between the *(u,d,s)* core and the hadronic envelope (Vogt et al. 2004). Vogt et al. (2004) found that in the CFL phase photon emission from pion annihilation dominates that from thermal e^+e^- annihilation (due to in-medium pion dispersion relations). Vogt et al. (2004) compared the energy flux from photons to that of neutrinos emitted (Reddy et al. 2003a,b) from a theoretical CFL quark star finding that the radiated energy from photon exceeds that from neutrinos by one to three orders of magnitude over a range of temperatures (∼5-30 MeV) and that photon flux from a newly born CFL quark star corresponds to that of a blackbody emitter.

Studying accretion onto a bare CFL quark star, Ouyed et al. (2005) found that the photon fireball energy generated via the conversion of accreted hadronic material into CFL quark matter (Vogt et al. 2004) translates into (0.01 - 1) $\mathrm{M}_{\odot} c^2 \mathrm{s}^{-1}$ of accretion energy. Analogously, during the final stages of the conversion from a neutron star to a CFL quark star, in the frame of the surface of the quark star matter is falling onto the star. This conversion is accompanied by a supersonic contraction that leaves a gap between what will become the remnant quark star and the outer layers of the neutron star and the photon fireball builds up in this gap. If $\sim 1\%$ of the emitted photons interact with the outer layers of the neutron star the photon fireball would be capable of accelerating neutron-rich matter to a Lorentz factor above 100 (Ouyed et al. 2005). At maximum efficiency the fireball can impart enough kinetic energy to eject up to 10^{-2} $\mathrm{M}_{\odot}$ (Ouyed et al. 2005), although we have found that for ejecta masses greater than $10^{-3} M_{\odot}$ the expansion would be non-relativistic. Further detailed dynamic analysis of local photon emission and out-of-equilibrium processes will provide more insight into the role of photon emission on possible mass ejection and will be carried out as future research.

Niebergal et al. (2010) carried out detailed hydrodynamic simulations of the conversion from neutron star to quark star on a much smaller length scale than other work done on the same topic (Herzog & Röpke 2011; Pagliara et al. 2013) and the results suggested that the conversion to *(u,d,s)* quark matter could be detonative. Niebergal et al. (2010) found that the burning front laminar speed was much faster (0.002c - 0.04c) than that derived using a reactive-diffusive description and that neutrino cooling would cause the burning front to stall at lower densities. These effects may allow for a flame wrinkling instability to form which could lead to detonation (Niebergal et al. 2010) and thus a QN explosion. The work carried out in Niebergal et al. (2010) represents the first step towards a hydrodynamic description of the QN. As will be discussed in Sect. 5.3 there are several avenues that must be considered before more definitive conclusions can be drawn on mass ejection by detonation.

3.2. *Timing*

The time scale for the conversion of the hadronic neutron star to a quark star is dependant on the central pressure of the neutron star and its gravitational mass (Berezhiani et al. 2003). It has been shown that for massive neutron stars that either the accretion of SN fall-back material or the spin-down evolution can cause the core density to exceed that of quark deconfinement, triggering a QN (Staff et al. 2006).

The length of time between SN and QN explosion ($t_{\rm delay}$), effectively the time it takes for the central density of the neutron star to exceed quark deconfinement, can vary from milliseconds to years (Berezhiani et al. 2003; Staff et al. 2006). Sagert et al. (2009) and Fischer et al. (2011) both considered a quark-hadron phase transition occurring in the early post-bounce phase of a core-collapse SN. The phase transition powers a strong shock that acts as a mechanism for triggering a SN explosion. For this work we consider much longer time delays (on the order of days to weeks) before the onset of the quark-hadron phase transition. This time delay plays a crucial role in determining the subsequent evolution of the stellar remnant. When the delay is short ($\lesssim 8$ days) the SN envelope is still dense and the energy of the impacting QN ejecta is used up spallating the inner region of the SN envelope (Ouyed et al. 2011). This leads to the destruction of ^{56}Ni and the formation of ^{44}Ti and results in a subluminous SN. The reduced luminosity is due to the lack of radioactive decay of ^{56}Ni (Ouyed et al. 2011). When the time delay is long (on the order of months or longer) the SN envelope will have become too diffuse to significantly interact with the QN ejecta. For massive QN ejecta with long time delays fall-back of the ejected material can occur which has implications for γ-ray bursts, soft γ-ray repeaters and anomolous X-ray pulsars (Ouyed et al. 2007a,b; Koning et al. 2012).

This work will focus on the scenario in which a SN is followed on the order of weeks by a QN. In this case, referred to as a dual-shock QN (dsQN), the expanded SN envelope is bombarded by the QN ejecta reheating the SN

envelope. The extended size and high temperature of the re-shocked SN envelope yields a brilliant radiance capable of reproducing the observed luminous peaks of SLSNe. As the radiation from the extended envelope fades, an inner region of mixed QN and SN material is revealed which can explain both the luminosity decay rate of SLSNe as well as curious spectral features.

4. DUAL-SHOCK QUARK NOVA

The evolution of a dsQN can be considered as three distinct phases; *delay, shock* and *cooling*. During the *delay* phase the SN envelope expands homologously ($v \propto r$) while the neutron star evolves towards a QN explosion. For fiducial values the radius of the SN envelope will reach $\sim 10^{15}$ cm during this phase. The end of the *delay phase* is marked by the detonation of the QN.

At the beginning of the *shock* phase the ultra-relativistic QN ejecta (Ouyed et al. 2005; Ouyed & Leahy 2009) quickly catches and slams into the inner edge of the SN envelope. This collision creates a shock front that propels through the SN envelope reheating it to a temperature $\sim 10^9$ K (Leahy & Ouyed 2008). As the shock progresses, the inner region of the re-shocked SN envelope mixes with the impacting QN ejecta to create a thin shell interior to the envelope, referred to as the hot plate in Ouyed et al. (2012) (furthermore: paper I).

The end of the *shock* phase and beginning of the *cooling* phase is defined to be the moment when the shock breaks out of the SN envelope. By this time the inner shell will be fully formed and slowly coasting inside of the shocked envelope. During the *cooling* phase both the envelope and the inner shell will cool via adiabatic expansion and radiative emission. Following the same methodology used in paper I, for the work presented here we model the light curves of dsQNe during their *cooling* phase.

4.1. *The Inner Shell*

As the QN ejecta ploughs through the SN envelope material builds up to form the inner shell. The momentum of the inner shell is equal to the sum of the initial momentum of the QN ejecta and that of all the SN material that is eventually swept up (which can be expressed as a velocity integral)

$$M_{\rm sh} v_{\rm sh} = \frac{E_{\rm QN}}{c} + \int_0^{v_{\rm sh}} v \frac{{\rm d}M_{\rm SN}}{{\rm d}v} {\rm d}v \tag{1}$$

where $E_{\rm QN}$ is the kinetic energy of the QN ejecta. Assuming that the density of the homologously expanding ($v \propto r$) SN envelope is homogeneously distributed, the SN mass interior to velocity v is given by

$$M(v) = M_{\rm SN} \left(\frac{v}{v_{\rm SN,max}} \right)^3 \tag{2}$$

where $M_{\rm SN}$ is the total mass and $v_{\rm SN,max}$ is the outer edge velocity of the SN envelope. Since the mass of the QN ejecta is negligible compared to that of

the swept up SN material we can substitute Eqn. 2 into Eqn. 1 and solve for $v_{\rm sh}$ giving;

$$v_{\rm sh} = \left(\frac{4 E_{\rm QN} v_{\rm SN,max}^3}{c M_{\rm SN}} \right)^{1/4} \tag{3}$$

The velocity of the inner shell that we found as a fit parameter in paper I was approximately 10% of our theoretically predicted value. Upon revisiting our derivation of R band luminosity used in paper I, we found that there was a missing factor of π and with this small correction the inner shell velocity used in this work is now in full agreement with the theoretical value (eqn. 3). The mass of the inner shell is given by;

$$m_{\rm sh} = \left(\frac{4 E_{\rm QN}}{c v_{\rm SN,max}} \right)^{3/4} M_{\rm SN}^{1/4} \, . \tag{4}$$

For this first-order description of the geometry of the inner shell we assume that processes such as turbulent mixing and reverse shocks cause the thickness ($\Delta R_{\rm sh}$) of the inner shell to remain constant once it has begun to coast (defined to begin at radius, $R_{\rm sh,0}$). We can use shock physics as a check of the physical parameters of the inner shell. Under the assumption of a strong shock the density behind the shock is four times that of the unshocked material. Considering a SN envelope of 30 $M_\odot$ at a radius of 10^{15} cm being shocked, the density behind the shock would be $\sim 10^{-10}$ g cm^{-3}. Now for fiduical values for the inner shell of $\Delta R_{\rm sh} = 2 \times 10^{13}$ cm, $R_{\rm sh,0} = 4 \times 10^{14}$ cm and $M_{\rm sh} = 3 M_\odot$ the density is $\sim 10^{-10}$ g cm^{-3}, which agrees with the expected value from shock physics. Emission from the inner shell is treated as diffusion luminosity in the same manner as was used in paper I.

The inner shell is fully parameterized by: temperature, mass, velocity, thickness and coasting radius. For our analysis of each SLSN target considered in this work we use the same coasting radius for the inner shell, namely the best fit value of $R_{\rm sh,0} = 4 \times 10^{14}$ cm that was found in paper I. The only parameter pertaining solely to the inner shell that we allow to be adjusted is shell thickness.

A detailed look at the formation of the inner shell using a full hydrodynamic treatment would help to understand how physical parameters of the inner shell are affected by changing initial conditions such as the time delay between SN and QN.

4.2. *The Envelope*

Fiducial values, found in paper I, for the shock speed ($v_{\rm shock} = 6000$ km s^{-1}) and the outer edge velocity of the homologously expanding ($v \propto r$) envelope ($v_{\rm SN,max} = 4100$ km s^{-1}) are used for the work presented here. By fixing $v_{\rm shock}$ and $v_{\rm SN,max}$ the variation in the time at which the *cooling* phase begins is uniquely determined by $t_{\rm delay}$. Following the same methodology as paper I, a simple temperature profile is considered for the envelope where

$T(r) \propto r^{-\beta}$ with $\beta = 0.2$. In this work the progenitor star mass ($M_\star$) is a free parameter and the mass of the inner shell ($M_{\rm sh}$) is prescribed by conservation laws, thus the mass of the envelope is found simply as $M_{\rm env} = M_\star - M_{\rm sh}$.

4.3. *Cooling*

Since the inner shell and the envelope are initially both parts of the same physical structure, namely the re-shocked SN envelope, they both start with same initial temperature (T_0). As the envelope and the inner shell expand they cool adiabatically, due to the difference in geometries (the envelope expanding spherically and the inner shell with constant thickness) they follow different cooling profiles. The temperature of the envelope evolves as $T_{\rm env}(t) \propto T_0\, t^{-2}$ and for the inner shell $T_{\rm sh}(t) \propto T_0\, t^{-4/3}$ (see paper I for derivation).

As continuum radiation is emitted by the envelope an equivalent amount of thermal energy is removed, thereby conserving energy. Since the *cooling* phase begins when the envelope is still relatively optically thick, radiative cooling starts at the outer edge of the envelope. Due to radiative cooling, over time a hot-cold interface progresses inward through the envelope. In our model once an outer layer of the envelope is radiatively cooled it no longer emits radiation. At the late stages of the dsQN light curve, radiative cooling will have caused the hot-cold interface to progress such that most of the envelope has been cooled. By this time the envelope has also expanded causing it to become more optically thin and thus making our optically thick radiative cooling approximation less valid. In reality as the envelope becomes more diffuse radiative cooling will cause the whole envelope to cool rather than just the outer layers and lead to an increase in the cooling rate of the envelope with time. The effect of this can be seen in the envelope contribution to the dsQN light curve (plotted as a blue dotted line in Fig. 1): as the change in slope around day 170 is due to the envelope remaining hotter than physically likely. Since the envelope is optically thin when this cooling artefact becomes significant, in most cases luminosity from the inner shell will already dominate the overall light curve rendering the problem moot. Rather than adding a more complicated radiative cooling law to our model we will simply note when the effect is seen during our fits to observations.

5. MODEL

For this work we use the astrophysical modelling software SHAPE, which allows us to construct the 3-D geometry of the dsQN scenario and perform radiative transfer (Wenger et al. 2012). We choose SHAPE over other radiative transfer codes for several reasons. First, the fast ray-tracing algorithm implemented in SHAPE allows us to quickly (within seconds) calculate the luminosity of the system. This is crucial when trying to find a best fit light curve involving several adjustable parameters. Other codes may take hours for a result, which would make the type of analysis presented in this paper impossible. Of course this speed comes with the cost of accuracy; we do

not consider multiple scattering. Second, the modelling environment within SHAPE is powerful and simple to use, making the construction of our model quick and robust. The temperature as well as the dimensions of the geometry are governed by the physics described in section 4.

5.1. *Radiative Transfer Parameters*

For this analysis the radiative transfer calculation follows the same methodology used in paper I in which for each frequency (ν) an emission and absorption coefficient are specified. The emission coefficient used for the envelope has the form

$$j_\nu = \frac{A\, n_{\rm e}^2}{T^{3/2}} e^{h\nu/kT} \tag{5}$$

where A is a multiplicative factor which is related to the underlying radiative process. For this analysis we chose to fix A over the filter passband of each studied SLSN. For the R band $A = 5 \times 10^5$, V band $A = 1 \times 10^6$, B band $A = 7 \times 10^4$, u band $A = 5 \times 10^5$. The variations required in A allude to an emission mechanism more complex than our approximation described by eqn. 5. Assuming local thermodynamic equilibrium[3] the absorption coefficient corresponding to our j_ν is found by means of the Planck function (B_ν) to be

$$k_\nu = \frac{j_\nu}{B_\nu} \tag{6}$$

We as well include a Thompson scattering term to equation 6 of the form

$$k_{\nu,{\rm TH}} = B\, n_{\rm e}\, \sigma_{\rm TH} \tag{7}$$

where $\sigma_{\rm TH}$ is the Thompson scattering cross-section and B is a multiplicative factor which represents the fraction of scattered light that is not scattered back into the beam. For this work we set $B = 5 \times 10^{-4}$, which is the same as that used in paper I. Further details on SHAPE and the radiative transfer calculation can be found in paper I.

5.2. *Fiducial Model Characteristics*

Before fitting the observed SLSNe light curves with the dsQN model we felt it would be informative to first explore the light curves of dsQNe in a more general sense. To this end we built a generic dsQN model with the following physical parameters: $M_\star = 25 M_\odot$, $T_0 = 2.5 \times 10^9$ K, $\Delta R_{\rm sh} = 3 \times 10^{13}$cm and $t_{\rm delay} = 15$ days. The light curve associated with this model is plotted as a red solid line in Fig. 1. The component of the light curve caused by emission from the envelope is plotted as a blue dotted line in Fig. 1 and the contribution from the inner shell is represented by the green dashed line. As can be seen

[3]We assume LTE simply to constrain the form of the absorption coefficient and tie it to the emission coefficient. If this was not the case, then we would have another free parameter to tune.

in Fig. 1 the broad peak in the dsQN light curve is due to radiation emitted from the envelope. As time progresses the envelope cools and becomes less dense causing a rapid drop in emission, this allows for radiation from the slowly coasting and thus slowly cooling inner shell to begin to shine through. The post-peak luminosity decay rate in the overall light curve of the dsQN is slowed due to emission from the inner shell. In the late stages of the dsQN light curve there can exist a plateau due to emission from the inner shell.

In this section we will investigate the effect on light curve morphology of varying the physical parameters of a dsQN. For comparative purposes in each of the panels in Fig. 2 the red solid line denotes the same light curve as the overall light curve seen in Fig. 1 (red solid line). Then in each panel of Fig. 2 one physical parameter is adjusted to show its effect on the light curve, the higher value is denoted by the blue dotted line and lower value by the green dashed line. Clock-wise starting from the upper-left panel of Fig. 2; varying $M_\star$ ($20M_\odot$, $25M_\odot$ and $30M_\odot$), varying T_0 (2×10^9K, 2.5×10^9K and 3×10^9K), varying $\Delta R_{\rm sh}$ (2×10^{13}cm, 3×10^{13}cm and 4×10^{13}cm) and varying $t_{\rm delay}$ (10 days, 15 days and 20 days).

As seen in the upper-left panel of Fig. 2 the effect of varying $M_\star$ is simply scaling the height of the peak, with higher mass yielding a higher peak. As the post-peak luminosity drops support by radiation from the underlying inner shell kicks in at the same time for each of the light curves. This convergence is caused by the fact that changing the mass of the envelope has no effect on the emission from the inner shell.

Changing T_0 of the dsQN (as seen in the upper-right panel of Fig. 2) as well acts to scale the height of the peak, however the height of the peak is inversely proportional to T_0 (due to the form of the emission coefficient, see eqn. 5). In the case of varying T_0 the support from the inner shell on the overall light curve begins at different times because temperature directly effects the amount of radiation that can be emitted by the inner shell. For higher T_0 the luminosity of the inner shell is greater and its effect on the overall light curve can be seen sooner.

As shown in Fig. 1 the effect on the dsQN light curve of radiation from the inner shell can only be seen in the late stages once emission from the envelope has faded sufficiently. Thus as expected the lower-right panel of Fig. 2 shows that changing $\Delta R_{\rm sh}$ only impacts the tail of the dsQN light curve. All things being equal, a thinner shell implies higher density and thus more intense emission from the inner shell. The effect of increased density causing increased radiation can be seen in the lower-right panel on Fig. 2 where the thinner $\Delta R_{\rm sh}$ light curve has a more prominent plateau.

The physical parameter that has the most dramatic effect on light curve morphology is $t_{\rm delay}$, which can be seen in the lower-left panel of Fig. 2. A shorter $t_{\rm delay}$ implies that the SN envelope is more dense when it is re-shocked which translates to higher peak in the light curve. The shorter $t_{\rm delay}$ also demands that the SN envelope is smaller when it is re-shocked, leading to significant adiabatic losses and a steep luminosity decay rate. The dsQN with

a longer $t_{\rm delay}$ can not achieve as high of a luminosity peak, however reduced adiabatic losses allow the light curve to remain at a higher relative brightness for a longer time when compared to a dsQN with a shorter $t_{\rm delay}$. Another effect of adjusting $t_{\rm delay}$ is to change the time of peak luminosity relative to the time of SN explosion. A longer $t_{\rm delay}$ dsQN will peak in brightness later in time due to the simple fact that the shock must traverse a larger envelope before it can break out.

From Fig. 2 it is clear that changing the value of $M_\star$, T_0 or $t_{\rm delay}$ all effect the height of the luminosity peak of the light curve of a dsQN. Our approximated emission coefficient (see eqn. 5) contains the free parameter A which as well directly effects the amount of radiation emitted in our model at any given time. Thus we can use A to gain a better visualization of the effect of changing each physical parameter ($M_\star$, T_0 and $t_{\rm delay}$) on the shape of the light curve. In Fig. 3 we perform the same comparison as shown in Fig. 2 with the addition that each light curve is rescaled using A such that the absolute magnitude of the light curve in the R band peaks at -22. By comparing the light curves in the upper two panels of Fig. 3 it is clear that neither changing $M_\star$ nor T_0 significantly affect the post-peak luminosity decay rate of the dsQN. As seen in the upper-left panel of Fig. 3 increasing the mass of the envelope marginally increases the breadth of the light curve peak but does not affect the slope. Turning to the upper-right panel of Fig. 3 one can see that increasing T_0 has the same effect on the morphology of the light curve peak as increasing $M_\star$. The only difference between adjusting $M_\star$ and T_0 is that the intensity of the radiation from the inner shell increases with T_0 causing the plateau to vary directly with T_0.

From Figures 2 and 3 we can see that varying T_0 and $M_\star$ effectively only act as scaling factors, with minimal effect on the luminosity decay rate of the light curve. Since the effect is virtually the same, for all our fits to observed SLSN light curves we choose to fix T_0 at 2.5×10^9K and allow $M_\star$ to vary. The lower-left panel of Fig. 3 displays the effect of varying the delay between SN and QN. As was shown in Fig. 2 increasing $t_{\rm delay}$ causes the peak luminosity to occur later with respect to the time of SN explosion. Another consequence of increasing $t_{\rm delay}$ is to slow down the luminosity decay rate of the post-peak light curve of a dsQN. As we have found in this analysis the only parameter that we can adjust in order to change the luminosity decay rate in the dsQN model is $t_{\rm delay}$.

5.3. *Model Limitations*

Running detailed stellar evolution code and full radiative transfer calculations at each time step (approximately 100 per model light curve) would make exploring parameter-space unfeasibly slow. We therefore chose to make simplifying assumptions such as; a SN envelope containing only one species, no multiple scattering and no stellar evolution code. This simplicity is encompassed in the unknown emission process (i.e. the inclusion of constants A and B in eqns.5 & 7). With more powerful computers in the future we will

be able incorporate the aforementioned complex features in order to test the validity of these assumptions.

The hydrodynamics of the conversion from a neutron star to a quark star is at this time not well understood. In the context of the QN as described in Ouyed et al. (2002) the conversion follows a two-step process whereby first the *(u,d,d)* quark matter is deconfined and then a phase transition to *(u,d,s)* matter occurs. The results of Niebergal et al. (2010) have suggested that the *(u,d,d)* to *(u,d,s)* conversion may be detonative. The next step in the hydrodynamic analysis of the QN is to expand the work of Niebergal et al. (2010) to three dimensions. In order to gain an understanding of possible mass ejection future simulations must explicitly include the hadronic envelope. This will allow us to answer such questions as how will mixing at the *(u,d,d)*-*(u,d,s)* interface affect heat transfer to the hadronic envelope and how does varying the equation of state for the hadronic matter and bag constants for the *(u,d,d)* matter affect the evolution of the system? This will allow us to draw better conclusions on whether mass will be ejected as well as its kinetic energy. Knowing these important features will allow us to make better predictions as to how the interaction between the QN ejecta and SN envelope will proceed.

The geometry of the scenario considered in this work represents a first order description (i.e. no asymmetries, thin spherical inner shell and thick spherical envelope) of the dsQN environment. Developing detailed 3D hydrodynamic simulations of the interaction between the QN ejecta and SN envelope will help us to understand the potentially complex structure expected in a dsQN. Once the hydrodynamics of the dsQN are better understood we can consider a more realistic treatment of SN composition and full radiative transfer calculations to try to fully understand the emission processes.

This work is a proof of concept analysis aimed to show that with a simple geometric and radiative transfer description the dsQN can provide enough energy to power SLSNe and can give an explanation for the range of observed light curve morphologies.

6. FITS TO OBSERVATIONS

For this work we have fit the light curve of eight SLSNe using the dsQN model. The parameters that we adjusted to fit each set of observations were; $t_{\rm delay}$, $\Delta R_{\rm sh}$ and $M_\star$. Of these three free parameters $t_{\rm delay}$ and $M_\star$ only significantly affect radiation from the envelope while $\Delta R_{\rm sh}$ only affects emission from the inner shell. As was shown in section 5.2, varying $M_\star$ or T_0 have the same effect on the dsQN light curve. Thus for simplicity we fixed $T_0 = 2.5 \times 10^9$ K and allowed $M_\star$ to vary between model fits. The best fit values of these parameters for each SLSNe surveyed can be found in Table 3. For each panel of Fig. 4 the observations are plotted with open circles and the best fit dsQN light curve is plotted as a red solid line. Fig. 5 displays each of the best fit dsQN light curves plotted on the same axes. From Fig. 5 it can be seen that for dsQNe in which an inner shell is formed (all but PTF09cnd and

PTF10cwr) the magnitude of the radiation from the inner shell is remarkably consistent.

6.1. *SN 2005ap*

The best fit progenitor mass for SN 2005ap was $28M_{\odot}$. The high peak absolute magnitude and fast luminosity decay rate of SN 2005ap required a short time delay ($t_{\rm delay} = 11.25$ days) dsQN to fit the observations (see top row left panel of Fig. 4). Since the observations of SN 2005ap were only carried out for approximately 35 days post-peak, the luminosity had not dropped enough to potentially see contribution from the inner shell. Thus we were unable to determine if an inner shell was present in the dsQN model of this SLSN.

6.2. *SN 2006gy*

In the proof-of-principle paper (Ouyed et al. 2012) the fits to SN 2006gy ignored a π factor in the R band magnitude calculation, the fits presented here take this into account and thus are more accurate. Our fit to the observed light curve of SN 2006gy is displayed in the top row middle panel of Fig. 4. A $30M_{\odot}$ progenitor star was used in our model and the broad peak of SN 200gy required a time delay of 17 days. The distinct plateau in the late stages of the light curve was fit using a inner shell 2×10^{13}cm thick.

6.3. *SN 2006tf*

Although the observations of SN 2006tf do not include the leading edge of the light curve, the slow luminosity decay rate demanded that the dsQN used in this fit have the longest time delay of all SLSNe modelled in this work ($t_{\rm delay} = 22.5$ days). A progenitor star of $26M_{\odot}$ was used in our fit and the late stages of the light curve is affected by contribution from an 4×10^{13}cm thick inner shell. Our fit to the observed light curve of SN 2006tf is found in the top row right panel of Fig. 4.

6.4. *SN 2007bi*

A plot of our fit to the light curve of SN 2007bi is displayed in the middle row left panel of Fig. 4. A progenitor star of $25.5M_{\odot}$ was used in our model and the delay between SN and QN that best fit the shape of the SN 2007bi light curve was $t_{\rm delay} = 18.5$ days. The late stage plateau of the light curve was fit in our dsQN model by radiation predominantly from a 2.5×10^{13}cm thick inner shell.

6.5. *SN 2008es*

The narrow peak of the light curve of SN 2008es was fit by dsQN of a $28M_{\odot}$ progenitor star with a time delay between SN and QN of 12.5 days. At approximately 100 days after SN explosion the light curve of SN 2008es begins to be supported by luminosity originating from a 3×10^{13}cm thick inner shell. A plot of our fit to the light curve of SN 2008es is displayed in the middle row middle panel of Fig. 4.

6.6. *SN 2008fz*

The combination of high peak luminosity and broad light curve made SN 2008fz require a $35M_{\odot}$ progenitor star and time delay of 20 days between SN and QN. Our dsQN fit to the light curve is found in the middle row right panel of Fig. 4. The late stages of the SN 2008fz light curve is supported by luminosity from a 5×10^{12}cm inner shell.

6.7. *PTF09cnd*

A plot of our fit to the light curve of PTF09cnd is displayed in the bottom row left panel of Fig. 4. The best fit parameters for PTF09cnd ($t_{\rm delay} = 17$ days and $M_{\star} = 31M_{\odot}$) are similar to that of SN 2006gy with one exception. For PTF09cnd we found that the inner shell had to be nearly 10 times thicker than that of SN 2006gy (2×10^{14} cm, or approximately two fifths of the initial radius of the inner shell) in order to fit the late stages of the light curve. This difference in inner shell geometry may be attributed to difference in the abundance of the inner SN envelope and higher order mixing effects related to specific dynamics of the QN/SN interaction. Another possible explanation for the reduced radiation from the inner shell at the late stages of the light curve of PTF09cnd is that the inner shell is cooling faster than the imposed $T \propto t^{-4/3}$ law. A larger cooling index would simply imply that the shell is expanding in thickness with time. A more detailed study of the hydrodynamics of the QN/SN interaction would help to further understand the formation process of the inner shell. The late stages of our dsQN model fit to PTF09cnd displays a change in slope which is an artefact of the radiative cooling approximation discussed in section 4.3.

6.8. *PTF10cwr / SN 2010gx*

Displayed in the bottom row middle panel of Fig. 4 is the dsQN model fit to the observed light curve of PTF10cwr. This SLSN displayed the narrowest light curve of all those studied in this work and thus was fit with the shortest time delay (7.5 days) dsQN. A $25M_{\odot}$ progenitor star was used in our best fit model and the light curve of PTF10cwr showed no sign of the presence of an inner shell. The late stages of our dsQN model fit to PTF10cwr displays a change in slope which is an artefact of the radiative cooling approximation discussed in section 4.3.

7. DISCUSSION

7.1. *Spectra*

In the case of SN 2006gy there exists numerous observations that detail its spectral evolution (Smith et al. 2010). Unfortunately for other SLSNe, study of the spectra is limited by the amount of observations available, which in many cases is one spectral observation around the time of peak brightness. As discussed in paper I, the dsQN can display an Hα signature in which the underlying broad structure of the line is caused by thermally broadened emission originating from the inner shell, and emission and absorption from the envelope result in a blue-side absorption feature. Fig. 6 displays a schematic representation of the line of sight evolution of the Hα line in a typical dsQN. Unique to the dsQN scenario the wings of the Hα line are caused by thermal broadening rather than velocity broadening (see right-most Hα line in Fig. 6), naturally accounting for the long-lasting breadth of the line. As the Hα line progresses through the hot component of the envelope a P Cygni profile is added to the structure of the line, this is displayed as the middle Hα line in Fig. 6. Finally the cold outer layer of the envelope adds absorption to the blue-side of the Hα line (seen in the left-most line plotted in Fig. 6).

By classification SN 2005ap, PTF09cnd and PTF10cwr do not display any prominent hydrogen lines. Although each of these SLSNe do show some indication of a weak Hα line near peak luminosity, as mentioned in the supplemental material associated with Quimby et al. (2011). Unfortunately the poor signal to noise (S/N) ratio eliminates any possibility of studying these weak lines. The two spectral observations of SN 2008fz each show a strong Hα line that resembles that of SN 2006gy (Drake et al. 2010). While the Hα lines display a broad underlying structure, the only spectral observation of SN 2008fz that is at an epoch which would show significant absorption by the envelope has the red-wing of the Hα line cut off. Without the red-side of the line there is no way of comparing the observations to our predicted dsQN Hα line. The spectra of SN 2008es contains broad Balmer lines which display a P Cygni profile however the poor S/N ratio of the observations inhibits any study of these lines (Gezari et al. 2009).

For our work in paper I we performed detailed analysis of the spectral evolution of the Hα line observed in SN 2006gy. The dsQN model was shown to provide a unique explanation for both the persistent broad structure of the line as well as the blue-side absorption feature seen in Hα of SN 2006gy. In this work we study the Hα line of two other SLSNe; SN 2006tf and SN 2007bi. For SN 2007bi the Hα line observed in the spectra 54 days after peak brightness (see upper left panel of Fig. 7) is mysterious as all other features of the spectra are consistent with a type Ic SN and thus should be free of hydrogen Gal-Yam et al. (2009). For comparative purposes we have plotted the Hα line observed in SN 2006gy (upper right panel of Fig. 7) from a similar epoch as the spectral observation of SN 2007bi. The bottom panel of Fig. 7 is the dsQN model Hα line from the same epoch (from paper I). Although

the S/N ratio of the SN 2007bi prevents the study of the delicate structure of the Hα line the large scale features are similar to that of a dsQN, namely the broad underlying structure and strong blue-side absorption.

The spectrum of SN 2006tf has multiple observations at different epochs along its light curve. As noted by Smith et al. (2008) the Hα line observed in SN 2006tf resembles that of SN 2006gy as it contains a broad underlying structure that becomes more prominent with time. The upper left panel of Fig. 8 displays an overplotting of four observations of the Hα line of SN 2006tf. For comparison the upper right panel of Fig. 8 displays an overplotting of four spectral observations of SN 2006gy from similar epochs. The bottom panel of Fig. 8 displays dsQN model Hα lines from roughly similar epochs as the observations of SN 2006tf and SN 2006gy. In the dsQN model Hα line and that of SN 2006tf and SN 2006gy there exists a broad component to the line as well as a blue-side absorption feature that diminishes in strength over time.

The differences in the Hα lines of SN 2006tf and SN 2007bi are consistent with the different $t_{\rm delay}$ of the dsQN description of these SLSNe. In the case of SN 2007bi the shorter time delay ($t_{\rm delay} = 18.5$ days) implies that the envelope is still dense at the time of spectral observation and thus there exists a strong blue-side absorption feature. As for SN 2006tf the time delay is significantly longer ($t_{\rm delay} = 22.5$ days) therefore the envelope is much more diffuse during the spectral observations and the blue-side absorption feature is weaker.

Interestingly the SLSNe with light curves that are best fit with dsQN models without inner shells (SN 2005ap and PTF10cwr) or with minimal influence from the inner shell (PTF09cnd) show no broad Hα features in late phase spectral observations (see supplemental material from Quimby et al. 2011). This is consistent with the dsQN explanation for the origin of the persistent broad Hα feature.

7.2. *The Envelope*

The mass of the envelope as well as the initial shock temperature both act only to scale up or down the peak of the dsQN light curve. We found that the only parameter capable of significantly changing the luminosity decay rate is the time delay between SN and QN. All SLSNe with X-ray observations show remarkably quiet X-ray production. This is expected in the context of a dsQN due to the cold outer layer of the envelope which would act as an efficient absorber of high energy radiation. The SN envelope is likely to be rich in metals such as carbon, oxygen, and magnesium (e.g. Nomoto et al. 2006). The presences of these heavier elements would provide greater X-ray absorption compared to a purely hydrogen envelope. The formulation that we used for radiative transfer coefficients (see eqn. 5 and 6) provided a good fit to each of the SLSN light curves that we studied. This could be an indication that the continuum emission mechanism for these SLSNe resembles recombination which has a similar form as eqn. 5. Further study of SLSNe in which the light curve was observed in several passbands would help to

determine the true temperature dependence for the emission coefficient and help in understanding the radiation mechanism.

7.3. *The Inner Shell*

Luminosity from the inner shell only begins to affect the shape of the light curves well past peak luminosity (typically once the luminosity has dropped to ~ -19.5 absolute magnitude). The slowing of the luminosity decay rate, or *plateauing* of the light curve in the late stage is caused by radiation from the inner shell shining through the diffuse envelope.

8. CONCLUSIONS AND PREDICTIONS

We have shown that the dsQN scenario can be used to explain the light curves of all eight SLSN targets studied. In the context of dsQNe, progenitor stars ranging between 25-35 $M_{\odot}$ provide ample energy to power the large radiated energy budget of SLSNe.

We found that the physical parameter with the greatest impact on dsQN light curve morphology was the time delay between SN and QN. Shorter time delay dsQN yield a peak magnitude that is higher and a faster luminosity decay rate (narrower light curve). While for longer time delays the peak magnitude is lower and the light curve is broader. A variation in time delay in the dsQN description provides an explanation for the wide variety of SLSN light curve morphology. From our analysis we found that for shorter time delay dsQN the inner shell may not be formed. The implication being that the energy that would go into forming the inner shell may instead be lost to pressure-volume work, however further study of the dynamics of the QN-SN interaction must be undertaken.

We have also examined the singular Hα spectral line profile found in three different SLSNe observations (SN 2006gy, SN 2006tf and SN 2007bi). The broad structure of the line is accounted for by thermally broadened emission from the inner shell, while the intermediate peak and blue-side absorption feature are due to contribution from the envelope. We found that the evolution of the blue-side absorption feature in the Hα line of SN 2006gy and SN 2006tf is consistent with diffusion of the envelope.

Unique to the dsQN scenario is the fact that any core collapse SN that leaves behind a massive neutron star can in turn undergo a QN explosion. This is due to the fact that the conditions of the interior of the progenitor star determine whether the neutron star could become susceptible to QN collapse. There is no correlation to the progenitor star envelope (for example whether or not hydrogen is present), thus we expect a wide variety of types of SN can become super-luminous due to re-brightening via a QN collision.

Also predicted by the dsQN model is the possibility of a unique chemical signature caused by the spallation of the SN envelope by the QN ejecta (both in relative abundances of certain elements and their spatial location) (Ouyed et al. 2011). Ouyed et al. (2011) studied the impact of spallation on chemical

abundances of SN remnants and the relationship between the density of the SN envelope during the QN interaction and the depth to which the spallation occurs within the SN envelope.

A dsQN is expected to emit two bursts of X-rays. The first X-ray emission event would occur when the shock from the original SN breaks out of the stellar envelope and the second analogously occurs for the QN shock break-out of the SN envelope. If the time delay between SN and QN is short then the X-ray bursts could in fact be overlapped leading to a broadened X-ray light curve. However if the time delay is long then there should be two distinct X-ray peaks.

This work is funded by the Natural Sciences and Engineering Research Council of Canada. N.K. would like to acknowledge support from the Killam Trusts. The authors would like to thank the anonymous referee for providing robust discussion on this work and for suggesting interesting avenues of future research.

REFERENCES

Alcock, C., Farhi, E., & Olinto, A. 1986, ApJ, 310, 261

Alford, M., Rajagopal, K., & Wilczek, F. 1999, Nuclear Physics B, 537, 443

Alford, M. G., Schmitt, A., Rajagopal, K., & Schäfer, T. 2008, Reviews of Modern Physics, 80, 1455

Arnett, W. D. 1982, ApJ, 253, 785

Berezhiani, Z., Bombaci, I., Drago, A., Frontera, F., & Lavagno, A. 2003, ApJ, 586, 1250

Blinnikov, S. I. 2008, in American Institute of Physics Conference Series, Vol. 1016, Origin of Matter and Evolution of Galaxies, ed. T. Suda, T. Nozawa, A. Ohnishi, K. Kato, M. Y. Fujimoto, T. Kajino, & S. Kubono, 241–248

Bodmer, A. R. 1971, Phys. Rev. D, 4, 1601

Bombaci, I. & Datta, B. 2000, ApJ, 530, L69

Bucciantini, N., Quataert, E., Metzger, B. D., Thompson, T. A., Arons, J., & Del Zanna, L. 2009, MNRAS, 396, 2038

Cheng, K. S. & Dai, Z. G. 1996, Physical Review Letters, 77, 1210

Chevalier, R. A. 1982, ApJ, 258, 790

—. 2012, ApJ, 752, L2

Chevalier, R. A. & Irwin, C. M. 2011, ApJ, 729, L6

—. 2012, ApJ, 747, L17

Dai, Z., Peng, Q., & Lu, T. 1995, ApJ, 440, 815

Dessart, L., Hillier, D. J., Waldman, R., Livne, E., & Blondin, S. 2012, MNRAS, 426, L76

Drake, A. J., Djorgovski, S. G., Mahabal, A., Beshore, E., Larson, S., Graham, M. J., Williams, R., Christensen, E., Catelan, M., Boattini, A., Gibbs, A., Hill, R., & Kowalski, R. 2009, ApJ, 696, 870

Drake, A. J., Djorgovski, S. G., Prieto, J. L., Mahabal, A., Balam, D., Williams, R., Graham, M. J., Catelan, M., Beshore, E., & Larson, S. 2010, ApJ, 718, L127

Fischer, T., Sagert, I., Pagliara, G., Hempel, M., Schaffner-Bielich, J., Rauscher, T., Thielemann, F.-K., Käppeli, R., Martínez-Pinedo, G., & Liebendörfer, M. 2011, ApJS, 194, 39

Fryer, C. L. 1999, ApJ, 522, 413
Gal-Yam, A., Mazzali, P., Ofek, E. O., Nugent, P. E., Kulkarni, S. R., Kasliwal, M. M., Quimby, R. M., Filippenko, A. V., Cenko, S. B., Chornock, R., Waldman, R., Kasen, D., Sullivan, M., Beshore, E. C., Drake, A. J., Thomas, R. C., Bloom, J. S., Poznanski, D., Miller, A. A., Foley, R. J., Silverman, J. M., Arcavi, I., Ellis, R. S., & Deng, J. 2009, Nature, 462, 624
Gezari, S., Halpern, J. P., Grupe, D., Yuan, F., Quimby, R., McKay, T., Chamarro, D., Sisson, M. D., Akerlof, C., Wheeler, J. C., Brown, P. J., Cenko, S. B., Rau, A., Djordjevic, J. O., & Terndrup, D. M. 2009, ApJ, 690, 1313
Ginzburg, S. & Balberg, S. 2012, ApJ, 757, 178
Grassberg, E. K., Imshennik, V. S., & Nadyozhin, D. K. 1971, Astro. & Space Sci., 10, 28
Herzog, M. & Röpke, F. K. 2011, Phys. Rev. D, 84, 083002
Itoh, N. 1970, Progress of Theoretical Physics, 44, 291
Iwamoto, N. 1980, Physical Review Letters, 44, 1637
Jaikumar, P., Prakash, M., & Schäfer, T. 2002, Phys. Rev. D, 66, 063003
Kasen, D. & Bildsten, L. 2010, ApJ, 717, 245
Kasen, D., Woosley, S. E., & Heger, A. 2011, ApJ, 734, 102
Kawabata, K. S., Tanaka, M., Maeda, K., Hattori, T., Nomoto, K., Tominaga, N., & Yamanaka, M. 2009, ApJ, 697, 747
Keränen, P., Ouyed, R., & Jaikumar, P. 2005, ApJ, 618, 485
Kiewe, M., Gal-Yam, A., Arcavi, I., Leonard, D. C., Emilio Enriquez, J., Cenko, S. B., Fox, D. B., Moon, D.-S., Sand, D. J., Soderberg, A. M., & CCCP, T. 2012, ApJ, 744, 10
Koning, N., Ouyed, R., & Leahy, D. 2012, ArXiv e-print 1205.4355
Law, N. M., Kulkarni, S. R., Dekany, R. G., Ofek, E. O., Quimby, R. M., Nugent, P. E., Surace, J., Grillmair, C. C., Bloom, J. S., Kasliwal, M. M., Bildsten, L., Brown, T., Cenko, S. B., Ciardi, D., Croner, E., Djorgovski, S. G., van Eyken, J., Filippenko, A. V., Fox, D. B., Gal-Yam, A., Hale, D., Hamam, N., Helou, G., Henning, J., Howell, D. A., Jacobsen, J., Laher, R., Mattingly, S., McKenna, D., Pickles, A., Poznanski, D., Rahmer, G., Rau, A., Rosing, W., Shara, M., Smith, R., Starr, D., Sullivan, M., Velur, V., Walters, R., & Zolkower, J. 2009, PASP, 121, 1395
Leahy, D. & Ouyed, R. 2008, MNRAS, 387, 1193
Miller, A. A., Chornock, R., Perley, D. A., Ganeshalingam, M., Li, W., Butler, N. R., Bloom, J. S., Smith, N., Modjaz, M., Poznanski, D., Filippenko, A. V., Griffith, C. V., Shiode, J. H., & Silverman, J. M. 2009, ApJ, 690, 1303
Moriya, T. J., Blinnikov, S. I., Tominaga, N., Yoshida, N., Tanaka, M., Maeda, K., & Nomoto, K. 2013, MNRAS, 428, 1020
Niebergal, B., Ouyed, R., & Jaikumar, P. 2010, Phys. Rev. C, 82, 062801
Nomoto, K., Tominaga, N., Umeda, H., Kobayashi, C., & Maeda, K. 2006, Nuclear Physics A, 777, 424
Olinto, A. V. 1987, Physics Letters B, 192, 71
Ouyed, R., Dey, J., & Dey, M. 2002, A&A, 390, L39
Ouyed, R., Kostka, M., Koning, N., Leahy, D. A., & Steffen, W. 2012, MNRAS, 3043
Ouyed, R. & Leahy, D. 2009, ApJ, 696, 562
Ouyed, R., Leahy, D., & Niebergal, B. 2007a, A&A, 473, 357
—. 2007b, A&A, 475, 63

Ouyed, R., Leahy, D., Ouyed, A., & Jaikumar, P. 2011, Phys. Rev. Lett., 107, 151103
Ouyed, R., Rapp, R., & Vogt, C. 2005, ApJ, 632, 1001
Pagliara, G., Herzog, M., & Röpke, F. K. 2013, Phys. Rev. D, 87, 103007
Pan, T., Loeb, A., & Kasen, D. 2012, MNRAS, 2979
Pastorello, A., Smartt, S. J., Botticella, M. T., Maguire, K., Fraser, M., Smith, K., Kotak, R., Magill, L., Valenti, S., Young, D. R., Gezari, S., Bresolin, F., Kudritzki, R., Howell, D. A., Rest, A., Metcalfe, N., Mattila, S., Kankare, E., Huang, K. Y., Urata, Y., Burgett, W. S., Chambers, K. C., Dombeck, T., Flewelling, H., Grav, T., Heasley, J. N., Hodapp, K. W., Kaiser, N., Luppino, G. A., Lupton, R. H., Magnier, E. A., Monet, D. G., Morgan, J. S., Onaka, P. M., Price, P. A., Rhoads, P. H., Siegmund, W. A., Stubbs, C. W., Sweeney, W. E., Tonry, J. L., Wainscoat, R. J., Waterson, M. F., Waters, C., & Wynn-Williams, C. G. 2010, ApJ Lett., 724, L16
Quimby, R., Castro, F., Mondol, P., Caldwell, J., & Terrazas, E. 2007a, Central Bureau Electronic Telegrams, 793, 1
Quimby, R. M., Aldering, G., Wheeler, J. C., Höflich, P., Akerlof, C. W., & Rykoff, E. S. 2007b, ApJ, 668, L99
Quimby, R. M., Castro, F., Gerardy, C. L., Hoeflich, P., Kannappan, S. J., Mondol, P., Sellers, M., & Wheeler, J. C. 2005, in Bulletin of the American Astronomical Society, Vol. 37, American Astronomical Society Meeting Abstracts, 171.02
Quimby, R. M., Kulkarni, S. R., Kasliwal, M. M., Gal-Yam, A., Arcavi, I., Sullivan, M., Nugent, P., Thomas, R., Howell, D. A., Nakar, E., Bildsten, L., Theissen, C., Law, N. M., Dekany, R., Rahmer, G., Hale, D., Smith, R., Ofek, E. O., Zolkower, J., Velur, V., Walters, R., Henning, J., Bui, K., McKenna, D., Poznanski, D., Cenko, S. B., & Levitan, D. 2011, Nature, 474, 487
Rau, A., Kulkarni, S. R., Law, N. M., Bloom, J. S., Ciardi, D., Djorgovski, G. S., Fox, D. B., Gal-Yam, A., Grillmair, C. C., Kasliwal, M. M., Nugent, P. E., Ofek, E. O., Quimby, R. M., Reach, W. T., Shara, M., Bildsten, L., Cenko, S. B., Drake, A. J., Filippenko, A. V., Helfand, D. J., Helou, G., Howell, D. A., Poznanski, D., & Sullivan, M. 2009, PASP, 121, 1334
Reddy, S., Sadzikowski, M., & Tachibana, M. 2003a, Phys. Rev. D, 68, 053010
—. 2003b, Nuclear Physics A, 714, 337
Sagert, I., Fischer, T., Hempel, M., Pagliara, G., Schaffner-Bielich, J., Mezzacappa, A., Thielemann, F.-K., & Liebendörfer, M. 2009, Physical Review Letters, 102, 081101
Shapiro, S. L. & Teukolsky, S. A. 1983, Black holes, white dwarfs, and neutron stars: The physics of compact objects
Smith, N., Chornock, R., Li, W., Ganeshalingam, M., Silverman, J. M., Foley, R. J., Filippenko, A. V., & Barth, A. J. 2008, ApJ, 686, 467
Smith, N., Chornock, R., Silverman, J. M., Filippenko, A. V., & Foley, R. J. 2010, ApJ, 709, 856
Smith, N., Li, W., Foley, R. J., Wheeler, J. C., Pooley, D., Chornock, R., Filippenko, A. V., Silverman, J. M., Quimby, R., Bloom, J. S., & Hansen, C. 2007, ApJ, 666, 1116
Smith, N. & McCray, R. 2007, ApJ, 671, L17
Son, D. T. 2002, ArXiv High Energy Physics - Phenomenology e-print hep-ph/0204199
Son, D. T. & Stephanov, M. A. 2000a, Phys. Rev. D, 62, 059902
—. 2000b, Phys. Rev. D, 61, 074012

Srednicki, M. & Susskind, L. 1981, Nuclear Physics B, 187, 93
Staff, J. E., Ouyed, R., & Jaikumar, P. 2006, ApJ Lett., 645, L145
Vogt, C., Rapp, R., & Ouyed, R. 2004, Nuclear Physics A, 735, 543
Weidemann, V. 1977, A&A, 59, 411
Wenger, S., Ament, M., Steffen, W., Koning, N., Weiskopf, D., & Magnor, M. 2012, Computing in Science and Engineering, 14, 78
Witten, E. 1984, Phys. Rev. D, 30, 272
Woosley, S. E. 2010, ApJ, 719, L204
Woosley, S. E., Blinnikov, S., & Heger, A. 2007, Nature, 450, 390
Xu, R. X., Zhang, B., & Qiao, G. J. 2001, Astroparticle Physics, 15, 101
Young, D. R., Smartt, S. J., Valenti, S., Pastorello, A., Benetti, S., Benn, C. R., Bersier, D., Botticella, M. T., Corradi, R. L. M., Harutyunyan, A. H., Hrudkova, M., Hunter, I., Mattila, S., de Mooij, E. J. W., Navasardyan, H., Snellen, I. A. G., Tanvir, N. R., & Zampieri, L. 2010, A&A, 512, A70
Yungelson, L. R., van den Heuvel, E. P. J., Vink, J. S., Portegies Zwart, S. F., & de Koter, A. 2008, A&A, 477, 223

Department of Physics and Astronomy, University of Calgary, Calgary, AB, Canada, T2N 1N4.
Instituto de Astronomía Universidad Nacional Autonoma de México, Ensenada, B.C., Mexico

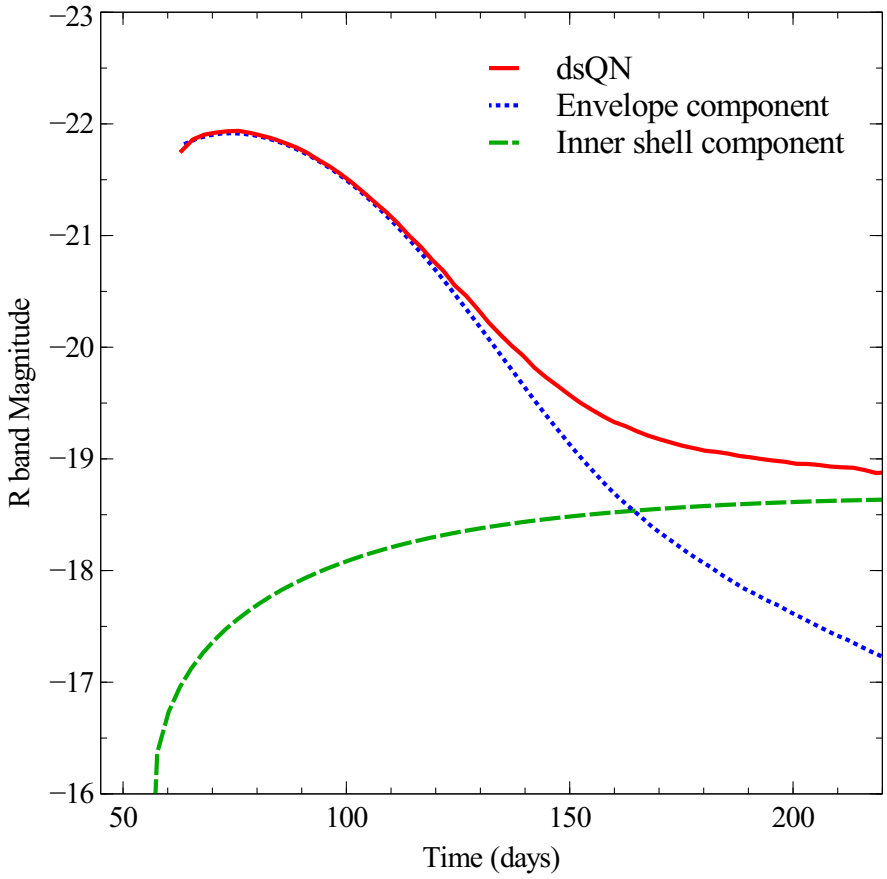

Fig. 1. Plotted as a red solid line is the R-band light curve of the dsQN. Radiation from the two components of the dsQN are also plotted. Radiation from the envelope is represented by the blue dashed line and that from the inner shell is denoted by the green dotted line.

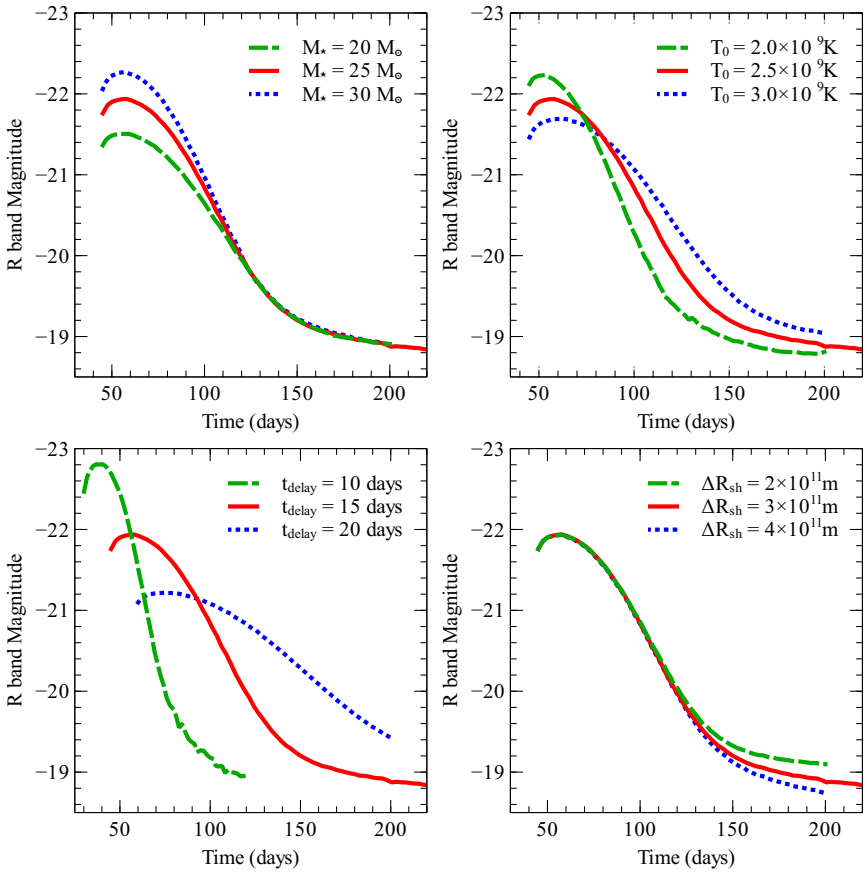

Fig. 2. In each panel the overlay of the R-band light curve of dsQN models with three different sets of physical parameters is plotted. For each panel one physical parameter is varied while the remaining parameters are held constant (values given in text). *Top-left: Mass of envelope ($M_\star$).* $M_\star = 20M_\odot$ (green dashed line), $M_\star = 25M_\odot$ (red solid line) and $M_\star = 30M_\odot$ (blue dotted line). *Top-right: Initial shock temperature (T_0).* $T_0 = 2 \times 10^9$ K (green dashed line), $T_0 = 2.5 \times 10^9$ K (red solid line) and $T_0 = 3 \times 10^9$ K (blue dotted line). *Bottom-left: Time delay between SN and QN ($t_{\rm delay}$).* $t_{\rm delay} = 10$ days (green dashed line), $t_{\rm delay} = 15$ days (red solid line) and $t_{\rm delay} = 20$ days (blue dotted line). *Bottom-right: Inner shell thickness ($\Delta R_{\rm sh}$).* $\Delta R_{\rm sh} = 2 \times 10^{11}$m (green dashed line), $\Delta R_{\rm sh} = 3 \times 10^{11}$m (red solid line) and $\Delta R_{\rm sh} = 4 \times 10^{11}$m (blue dotted line).

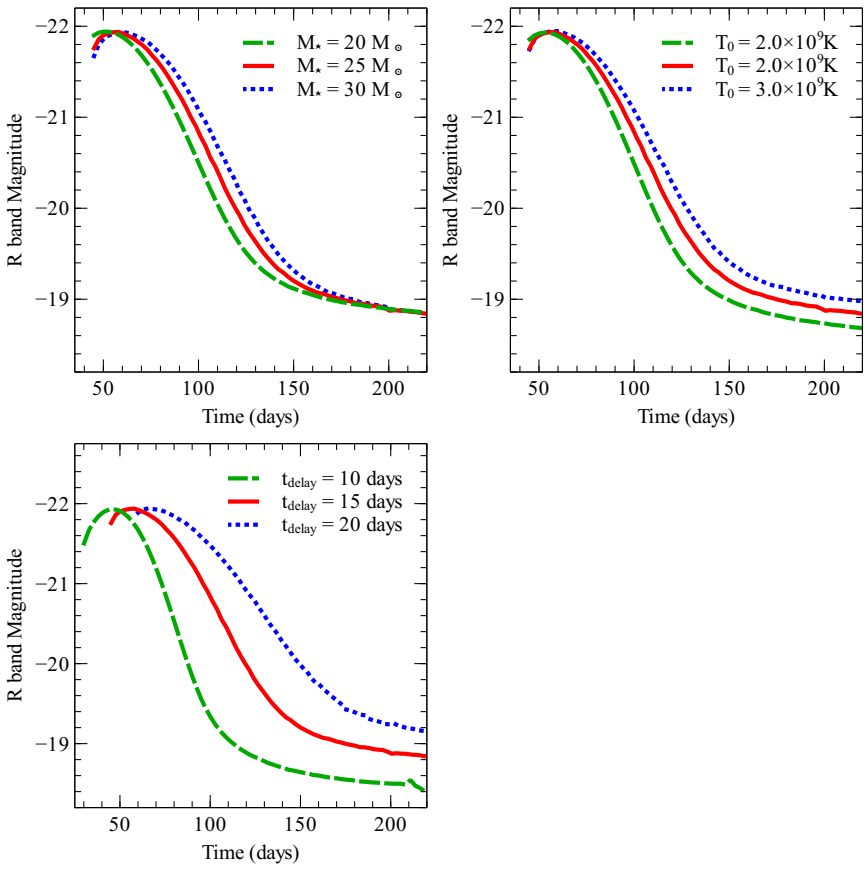

Fig. 3. In each panel the overlay of the R-band light curve of dsQN models with three different sets of physical parameters is plotted. Each light curve is scaled using the radiative transfer parameter A such that the peaks reach the same absolute magnitude. For each panel one physical parameter is varied while the remaining parameters are held constant (values given in text). *Top-left: Mass of envelope ($M_\star$).* $M_\star = 20M_\odot$ (green dashed line), $M_\star = 25M_\odot$ (red solid line) and $M_\star = 30M_\odot$ (blue dotted line). *Top-right: Initial shock temperature (T_0).* $T_0 = 2\times10^9$ K (green dashed line), $T_0 = 2.5\times10^9$ K (red solid line) and $T_0 = 3\times10^9$ K (blue dotted line). *Bottom-left: Time delay between SN and QN ($t_{\rm delay}$).* $t_{\rm delay} = 10$ days (green dashed line), $t_{\rm delay} = 15$ days (red solid line) and $t_{\rm delay} = 20$ days (blue dotted line).

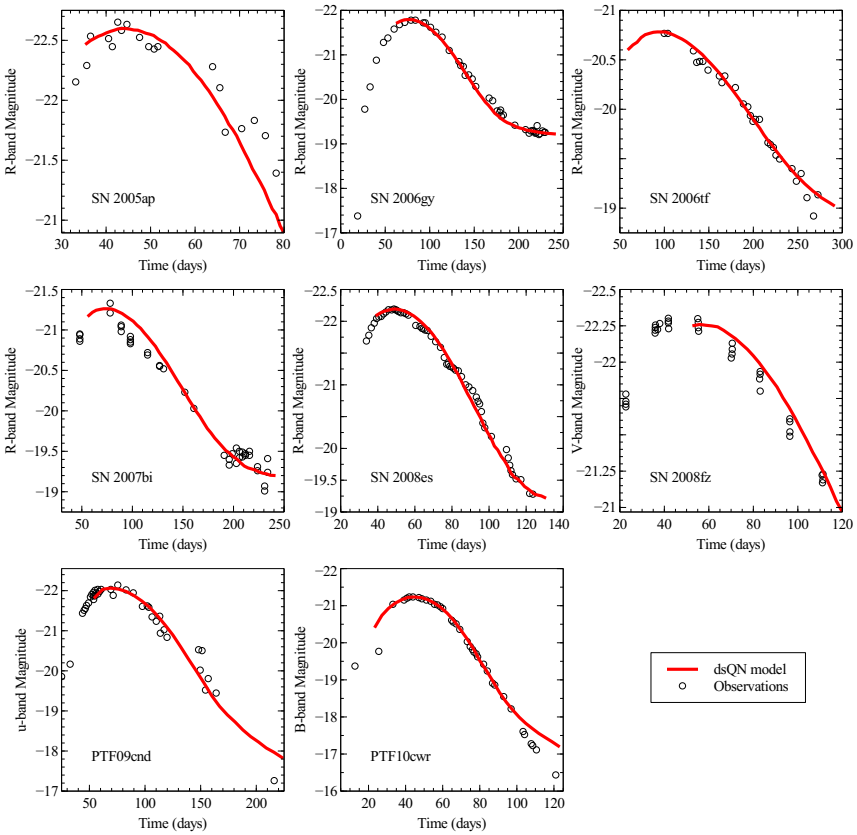

Fig. 4. For each panel the observed light curve is plotted with open black circles and the dsQN model is plotted as a solid red line. Time since the inferred SN explosion is plotted along the horizontal axis and the absolute magnitude in the observed band is plotted on the vertical axis. The best fit parameters used to generate these fits can be found in Table 3. From left-to-right and top-to-bottom the panels represent: SN 2005ap, SN 2006gy, SN 2006tf, SN 2007bi, SN 2008es, SN 2008fz, PTF09cnd and PTF10cwr.

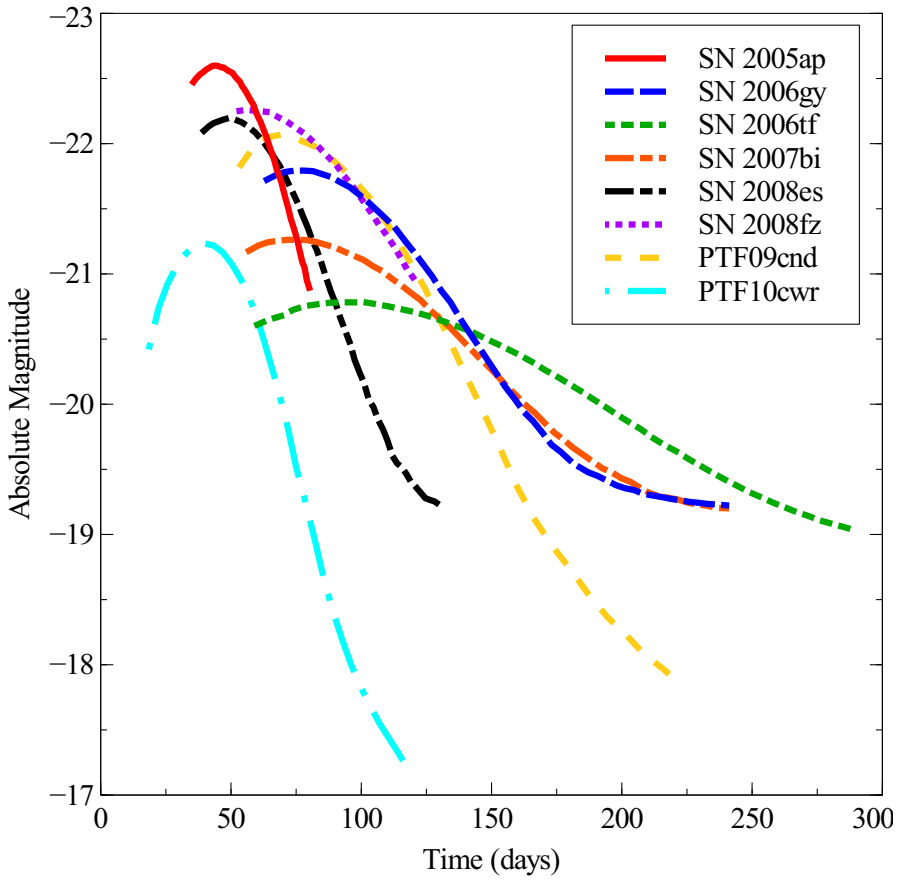

Fig. 5. The best fit dsQN model light curve for each of the SLSNe studied in this work are plotted on the same axis.

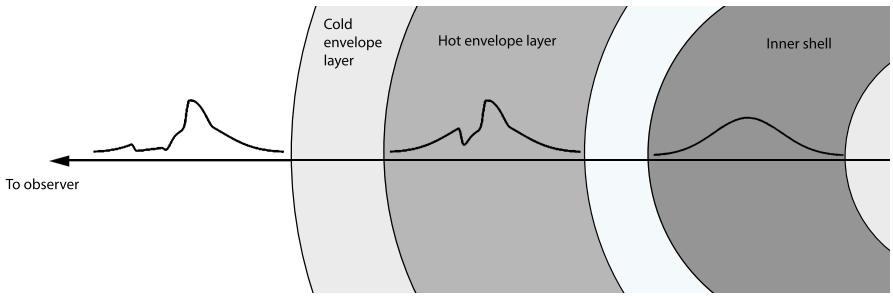

Fig. 6. The three Hα emission lines plotted here represent the Hα line at three different stages of its line of sight evolution. In the background a not-to-scale cartoon representation of the physical structure that contributes to the given emission line. The far right Hα line is thermally broadened emission from only the inner shell. The broad structure of the middle Hα line is emission from only the inner shell, while the hot envelope contributes a P Cygni profile on top of the broad structure. The far left Hα line is emission from the entire dsQN along the line of sight. The radiatively cooled outer layer adds increased blue-side absorption to the Hα line.

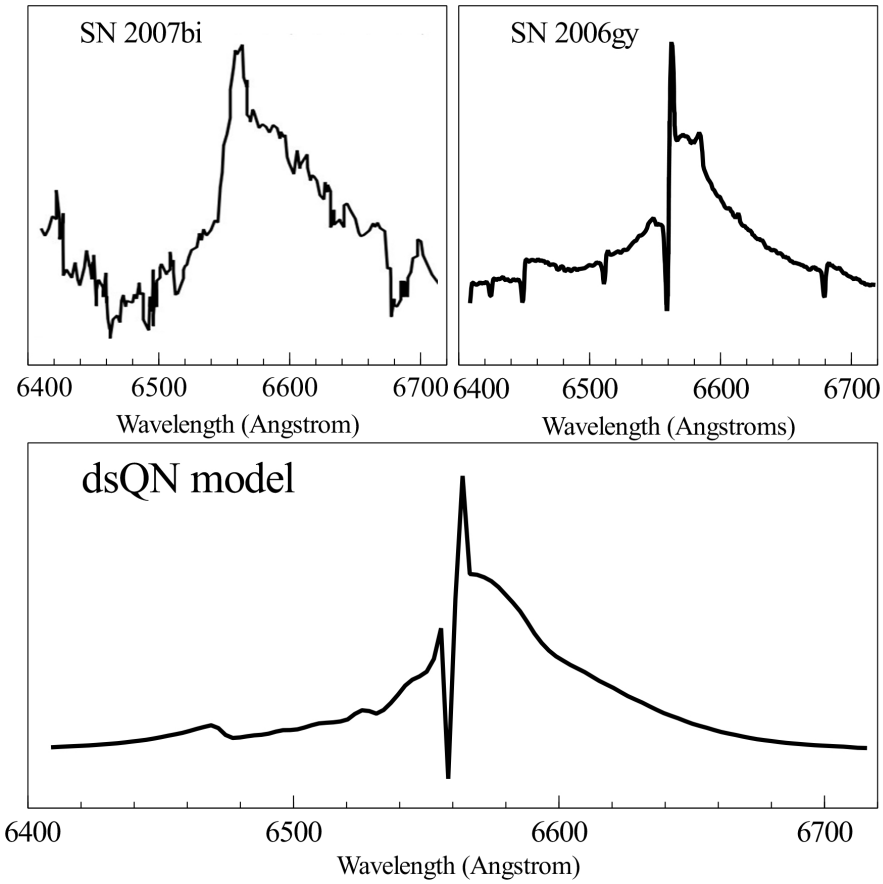

Fig. 7. Comparison of Hα line from spectra of SN 2006gy, SN 2007bi and the dsQN model. *Top-Left:* Plotted is the observed Hα line of SN 2007bi approximately 54 days after peak luminosity, data from Gal-Yam et al. 2009. *Top-Right:* The Hα line from the spectrum of SN 2006gy observed at approximately 50 days post-peak luminosity, data from Smith et al. 2010. *Bottom:* The dsQN model Hα line 50 days post-peak luminosity, from paper I.

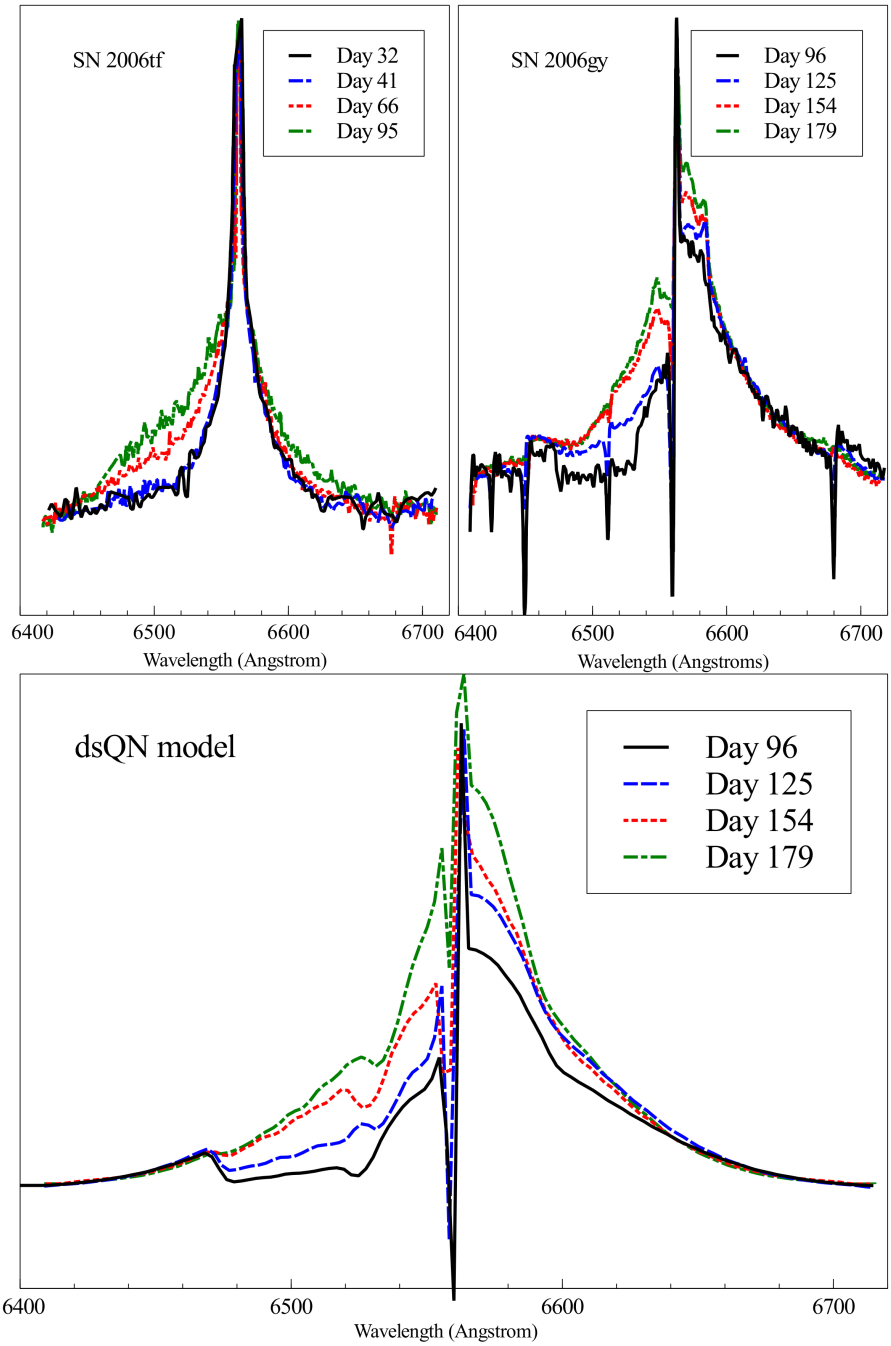

Fig. 8. Comparison of evolution of Hα line from SN 2006tf spectra, SN 2006gy and our dsQN model Hα line evolution. *Top-Left:* Plotted is an overlay of spectral observations of the Hα line observed in SN 2006tf (data from Smith et al. 2008). The observations are from; 32 (black solid line), 41 (blue dash line), 66 (red dotted line) and 95 (green dash-dot line) days after the first observation. *Top-Right* An overlay of Hα spectral lines from SN 2006gy is plotted, data from Smith et al. 2010. The Hα lines plotted are from days; 96 (black solid line), 125 (blue dashed line), 154 (red dotted line) and 179 (green dash-dot line) after the inferred SN explosion date. *Bottom:* Plotted is an overlay of the dsQN model Hα line that was used to fit the observations of SN 2006gy in paper I. The Hα lines plotted are from days; 96 (black solid line), 125 (blue dashed line), 154 (red dotted line) and 179 (green dash-dot line) after the inferred SN explosion date.

TABLE 1

COMPARISON OF PROPOSED SLSNE MODELS.

	Model			
SLSNe Property	PISN	CSM	Magnetar	dsQN
Energy Mechanism	$\gamma = 4/3$ instability[a]	Binary merger[b]	Rotational energy[c]	QN explosion [d]
Radiation Mechanism	Collision of ejecta[a]	CSM/SN interaction[e]	Synchrotron[c]	QN/SN interaction[d]
Progenitor mass ($M_\odot$)	313[f] - 1250[f]	100+[g]	8[h] - 25[i]	20[j] - 40[j]
X-rays	suppressed[k]	suppressed[l]	not discussed	suppressed[j]
Hydrogen in Spectra	unlikely[m]	necessary[n]	not discussed	likely[j]
Cause of long-lasting broad lines	not expected[o]	velocity of SN[g]	velocity of inner shell[p]	temperature of inner shell[j]
Late stage luminosity	radioactivity[a]	opaque outer region of CSM[q]	inner bubble[c]	inner shell emission[j]

[a]Woosley et al. (2007), [b]Chevalier (2012), [c]Kasen & Bildsten (2010), [d]Leahy & Ouyed (2008), [e]Chevalier (1982), [f]Pan et al. (2012), [g]Smith et al. (2010), [h]Weidemann (1977) [i]Fryer (1999), [j]Ouyed et al. (2012), [k]Blinnikov (2008), [l]Chevalier & Irwin (2012), [m]Yungelson et al. (2008), [n]Quimby et al. (2011), [o]Kasen et al. (2011), [p]Dessart et al. (2012), [q]Chevalier & Irwin (2011),

TABLE 2

LIST OF SLSNE TARGETS.

Name	Type	Peak Magnitude	Proposed Models
SN 2005ap	H-poor SLSN[a]	-22.7[b]	CSM[a], PISN[a],dsQN[c]
SN 2006gy	IIn[d]	-22 [e]	PISN[f], CSM[e], dsQN[c,g]
SN 2006tf	IIn[h]	$\sim$-20.8[h]	CSM[h]
SN 2007bi	Ic[i]	-21.3[i]	CC[j], PISN[i]
SN 2008es	II-L[k]	-22.2[k]	CSM[k]
SN 2008fz	IIn[l]	-22.3[l]	none[l]
PTF09cnd	H-poor SLSN[a]	-22[a]	CSM[a], PISN[a]
PTF10cwr	H-poor SLSN[a]	-21.2[m]	CSM[a], PISN[a]

[a] Quimby et al. (2011), [b] Quimby et al. (2007b), [c] Leahy & Ouyed (2008), [d] Quimby et al. (2005), [e] Smith & McCray (2007), [f] Woosley et al. (2007), [g] Ouyed et al. (2012), [h] Smith et al. (2008), [i] Gal-Yam et al. (2009), [j] Young et al. (2010), [k] Gezari et al. (2009), [l] Drake et al. (2010), [m] Pastorello et al. (2010)

TABLE 3

COMPARISON OF DSQN MODEL PARAMETERS USED TO FIT EACH SLSNE.

SLSNe	Time Delay ($t_{\rm delay}$) [days]	Mass ($M_\star$) [$M_\odot$]	Shell Thickness ($\Delta R_{\rm sh}$) [10^{13} cm]
SN 2005ap	11.25	28	N/A
SN 2006gy	17.0	30	2.0
SN 2006tf	22.5	26	4.0
SN 2007bi	18.5	25.5	2.5
SN 2008es	12.5	28	3.0
SN 2008fz	20.0	35	0.5
PTF09cnd	17.0	31	$\gtrsim 20$
PTF10cwr	7.5	25	N/A